

Fuzziness-based Spatial-Spectral Class Discriminant Information Preserving Active Learning for Hyperspectral Image Classification

Muhammad Ahmad

Abstract—Traditional Active/Self/Interactive Learning for Hyperspectral Image Classification (HSIC) increases the size of the training set without considering the class scatters and randomness among the existing and new samples. Second, very limited research has been carried out on joint spectral-spatial information and finally, a minor but still worth mentioning is the stopping criteria which not being much considered by the community. Therefore, this work proposes a novel fuzziness-based spatial-spectral within and between for both local and global class discriminant information preserving (FLG) method. We first investigate a spatial prior fuzziness-based misclassified sample information. We then compute the total local and global for both within and between class information and formulate it in a fine-grained manner. Later this information is fed to a discriminative objective function to query the heterogeneous samples which eliminate the randomness among the training samples. Experimental results on benchmark HSI datasets demonstrate the effectiveness of the FLG method on Generative, Extreme Learning Machine and Sparse Multinomial Logistic Regression (SMLR)-LORSAL classifiers.

Index Terms—Hyperspectral Image Classification (HSIC); Active Learning (AL); Fuzziness; Class Scatter; SVM; KNN; ELM; SMLR-LORSAL;



1 INTRODUCTION

HYPERSPECTRAL IMAGING (HSI) is concerned with the extraction of meaningful information from the objects of interest-based on the radiance acquired by the sensor from long, medium or short distance [1]. HSI technology has been investigated in a wide variety of urban, mineral exploration, environmental, in-depth classification of forest areas, monitoring the pollution in city areas, investigating the coastal and domestic water zones, inspection for natural risks, i.e. flood, fires, earthquakes, eruptions [2], [3].

Therefore, to enhance the applicability, robust, effective and automatic Hyperspectral Image Classification (HSIC) methods are required. The classical kernel-based methods [4] are effective and robust. Nevertheless, these methods are inadequate to handle ill-posed conditions [5]. Furthermore, it is well established fact that the HSIC performance depends on the quality and size of training data [6]. How-

ever, in the scenario of limited training samples, classical HSIC methods do not perform well [7], [8]. Therefore, the main objective of this work is to develop a novel method to automatically extract the meaningful information captured by HSI sensors particularly in the case when the labeled training samples are not adequate or not fully reliable [9]. In a nutshell, the following specific contributions are made in this work.

- 1) FLG utilizes the fuzziness concept instead of uncertainty and couples it with the samples diversity while maximizing separability measure using total local and global for both within and between class discriminant information.
- 2) Total global class information impairs the local topology and cannot satisfactorily characterize the local class discriminant information. This may lead to instability of within-class compact representation.
- 3) A similar problem whereby local class discriminant information only considers local between and within-class information and ignore the global class information.

• Department of Computer Engineering, Khwaja Fareed University of Engineering and Information Technology, Rahim Yar Khan, 64200, Pakistan.
E-mail: mahmad00@gmail.com

Manuscript received May 28, 2020.

- 4) To overcome the above two problems, we define a novel objective function that jointly considers the total global and local class discriminative information. The proposed discriminative objective function assesses the stationary behavior of samples in the spectral domain in a fine-grained manner.

The objective function proposed in this work is adapted for deriving a set of spatially heterogeneous samples that jointly optimize the above terms. The objective function is based on the optimization of a multi-objective problem for the estimation of within and between class scatters while preserving the total local and global class discriminant information. Thus, FLG significantly increases the generalization capabilities and robustness of classical machine learning classifiers.

The rest of the paper is structured as follows. Section 2 examines the related works. Section 3 presents the theoretical aspects of *FLG*. Section 4 discusses the details of experimental settings. Section 5 provides the details about HSI datasets, experimental results and comparison with the state-of-the-art methods. Finally, section 6 summarizes the contributions and discuss future research directions.

2 RELATED WORK

In the last decade, kernel-based methods have been successfully applied for HSIC. However, kernel-based methods do not perform well when the ratio between the number of labeled training samples and spectral bands [10], [11], [12] is small [13]. Several alternative methods have been proposed to address the issues related to the limited availability of labeled training samples. One of them is to iteratively enlarge the original training set in an interactive process, i.e, human-human interaction or human-machine interaction [14].

Active Learning (AL) is an iterative process of selecting informative samples from a set of unlabeled samples. The selection choice is based on a ranking of scores that are computed from a model's outcome. Carefully selected samples are added to the training set and the classifier is retrained with the new training set. The training with selected samples is robust because it uses samples that are suitable for learning. Thus, the sample selection criteria are a key component of the AL framework [1], [15]. The most common sample selection criteria are formalized into three different groups.

- 1) Uncertainty of samples [16], [17] and query by committee [18], [19]
- 2) Influence on the model such as length of gradients [20] and Fisher information ratio [21].
- 3) Intrinsic structure and distribution of the unlabeled samples such as Gaussian similarity [22], Kullback-Leibler divergence similarity [23], manifold learning [24], clustering [25] and density-weighting [26] methods.
- 4) AL combined with a special classifier such as AL combined with Logistic Regression [27], SVM [28] and Gaussian process regression [29].

These sample selection methods have shown that the AL process significantly improves the performance of any classifier while querying the informative samples [30]. However, in HSIC, the collection and labeling of queried samples are associated with a high cost in terms of time. Therefore, most of the previous studies focused on selecting the single sample in each iteration (stream-based), by assessing its uncertainty [31]. This can be computationally expensive because the classifier has to be retrained for each new labeled sample.

Pool-based (Batch-mode) methods have been proposed to address the above-mentioned issues by assessing the pool of samples. The major drawback of multiclass pool-based models is that the pool of selected samples brings redundancy i.e., no new knowledge or information is provided to the classifier in the retraining phase.

This work addresses the above-mentioned issues by defining a multiclass fuzziness-based total local and global for both within and between-class scatter information preserving AL pipeline. This work explicitly considers spatial-spectral heterogeneity of the selected samples by defining a novel discriminative objective function and properly generalize it. The combination of the above criteria results in the choice of the potentially most informative and heterogeneous samples than ever possible. The proposed method is experimentally compared with state-of-the-art methods and based on the comparisons, some guidelines are derived to use AL techniques for HSIC.

3 METHODOLOGY

A number of sample selection methods for AL have been proposed in the literature [7], [32], [33],

[34] though uncertainty ¹-based sample selection remains popular due to its simplicity. The probabilistic classification models can directly be used to compute the uncertainty whereas it's not that simple for non-probabilistic models [35].

Let us assume a HSI cube can be represented as $X = [x_1, x_2, x_3, \dots, x_L]^T \in \mathcal{R}^{L \times (M \times N)}$ composed of $(M \times N)$ samples per band belonging to C classes and L bands [36], [37], [38]. Further assume that (x_i, y_j) be a sample of Hyperspectral cube in which y_j is the class label of x_i sample. We first randomly select n number of labeled training samples to form a training set X_T and rest has been selected for the test set X_V . We further make sure that $n \ll m$ and $X_T \cap X_V = \emptyset$ [1] for each iteration of our proposed AL method.

3.1 Fuzziness

A probabilistic/non-probabilistic classifier produces the output $\mu = \mu_{ij}$ of $m \times C$ matrix containing probabilistic/non-probabilistic outputs. There is no need to compute the marginal probabilities for probabilistic classifiers however it is mandatory for non-probabilistic classifiers and for that discriminative random field is used to compute the probabilities. These probabilistic outputs are used to construct a membership matrix which must satisfy the properties [1], [7] $\sum_{j=1}^C \mu_{ij} = 1$ and $0 < \sum_{i=1}^N \mu_{ij} < 1$ where $\mu_{ij} = \mu_j(x_i) \in [0, 1]$ represent the membership of x_i to the y_j class. Later this membership matrix is used to compute the fuzziness of m samples for C class as;

$$E(\mu) = \frac{-1}{C} \sum_{i=1}^N \sum_{j=1}^C [\mu_{ij} \log(\mu_{ij}) + (1 - \mu_{ij}) \log(1 - \mu_{ij})] \quad (1)$$

3.2 Fuzziness Categorization

We first make a matrix of fuzziness information associated with samples' spatial information and their predicted and actual class labels and a test set, i.e., $[E(\mu), X_V(s), y_j(a), y_j(p), X_V]$ where $X_V(s)$ stands for spatial information of test set, $y_j(a)$ and $y_j(p)$ represents the actual and predicted class labels. Later a median-based fuzziness categorization method is proposed to select the samples to compute the class scatter information. There are two

ways to compute the median value to make \mathcal{F}_1 and \mathcal{F}_2 sets depending on the number of total samples. If the total number of samples is odd then the median can be computed as:

$$\mathcal{M}(\mathcal{F}_1) = \frac{m_1 + 1}{2} \quad (2)$$

$$\mathcal{M}(\mathcal{F}_2) = \frac{m_2 + 1}{2} \quad (3)$$

If the total number of samples in the test set is even then the median can be computed as;

$$\mathcal{M}(\mathcal{F}_1) = \frac{\frac{m_1}{2} + \frac{m_1+1}{2}}{2} \quad (4)$$

$$\mathcal{M}(\mathcal{F}_2) = \frac{\frac{m_2}{2} + \frac{m_2+1}{2}}{2} \quad (5)$$

where m_1 and m_2 refers to the total number of samples in \mathcal{F}_1 and \mathcal{F}_2 respectively. Now we have two sets of fuzziness then we will find the median values in both sets and keep these values in \mathcal{Q}_1 and \mathcal{Q}_2 . By this process, we create two fuzziness groups and place the samples in low ($[0 - 0.5]$ fuzziness magnitude) and high ($[0.5 - 1.0]$ fuzziness magnitude) fuzziness groups, respectively. From these two sets we select misclassified foreground samples to compute the local and global class discriminate information to select the heterogeneous spectral samples for the training set.

3.3 Global Class Discriminant Information

The fuzziness categorization process returns $\mathcal{X} = \{(x_i \mid i = 1, \dots, \mathcal{K} \text{ and } y_j \mid j = 1, \dots, C)\}$, where $x_i \in \mathcal{R}^{L \times (M \times N)}$, $\mathcal{K} < m$ and $n \ll \mathcal{K}$. The global class discriminant information preserving process aims to attain a space $\mathcal{R}^{L \times (M \times N)}$ in which each training sample x_i can be well represented by $x_i \rightarrow y_j \in \mathcal{R}^{L \times (M \times N)}$. Therefore, linear discriminant analysis (LDA) is most efficient method to preserve the global information in computational efficient fashion. LDA seeks a linear projection matrix $\mathbf{U} \in \mathcal{R}^{L \times (M \times N)}$ that maximizes the Fisher discriminant ratio (FDR) as follows:

$$\mathbf{U} = \underset{\mathbf{U}}{\operatorname{argmax}} \frac{|\mathbf{U}^T S_B \mathbf{U}|}{|\mathbf{U}^T S_W \mathbf{U}|} \quad (6)$$

where $S_B, S_W \in \mathcal{R}^{L \times L}$ are the global between and within class scatter matrices respectively.

The performance of FDR is highly dependent on the quality of the scatter matrices i.e. when the number of samples in each class is much smaller

1. Most uncertain sample has similar posteriori probability for two possible classes.

than the number of bands, S_W would be singular. This makes the inverse of S_W and the eigenvalue decomposition $S_W^{-1}S_B$ impracticable which is commonly known as small sample size problem [39]. However, non-probabilistic LDA (NPLDA) [40] and probabilistic vector-based LDA (PLDA) [41] methods have been proposed to address the problems. In NPLDA, regularized LDA (RLDA) use PCA to reduce the dimensionality of HSI from L to $L^* < L$ and performs the classical LDA. Therefore, the size of within-class scatters matrix S_W is reduced from $L \times L$ to $L^* \times L^*$, making S_W well-conditioned in the PCA subspace as long as L^* is small enough. Although PCA+LDA solves the singularity problem with the expense to lose geospatial information due to the lossy compression of PCA.

RLDA can hardly extract meaningful information when the size of the training samples becomes large. Unlike NPLDA counterparts, PLDA solves the singularity problem by capturing between and within-class variation under the probabilistic framework. Whereas, NPLDA extracts meaningful information by manipulating the scatter matrices. While the PLDA avoids the inverse of ill-conditioned S_W through probabilistic modeling of within and between class variation, individually. Moreover, since it explicitly characterizes both the class and noise components, PLDA has a unique advantage in capturing discriminative information. It may be discarded or considered as less important by its NPLDA counterparts [41].

Since NPLDA and PLDA successfully address the singularity problem of LDA, however, these are still far from solving the small sample size problem. In real-life, many HSI datasets are in the form of tensors and tensor structures are useful in alleviating the small sample size problem. Vectorization or reshaping consequently breaks the valuable tensor structures. To cope with these issues, multi-linear LDA (MLDA) approaches have been proposed to gain more robustness. According to different criteria used in projection learning, MLDA can be grouped into two categories, i.e. ratio-based MLDA (RMLDA) [42] and difference-based MLDA [43].

RMLDA consider $\mathcal{X} = \{\{\mathbf{x}_{ij} \in \mathcal{R}^{L_c \times L_r}\}_{i=1}^n\}_{j=1}^C$ as a set of true class HSI samples obtained by fuzziness process. The aim of RMLDA is to find projections that maximize the ratio between and within class scatter. For instance, 2D-RMLDA learn two matrices $U_r \in \mathcal{R}^{L_r \times q_r}$ and $U_s \in \mathcal{R}^{L_s \times q_s}$, which characterize the column and row spaces respectively. These matrices solved alternately based on the following scatter ratio criterion. By fixing U_r , U_s is solved by:

$$U_c = \operatorname{argmax}_U \frac{\operatorname{tr}(U^T S_{B_s} U)}{\operatorname{tr}(U^T S_{W_s} U)} \quad (7)$$

where $S_{W_s} \in \mathcal{R}^{L_s \times L_s}$ and $S_{B_s} \in \mathcal{R}^{L_s \times L_s}$ are the ML-DAs within and between class scatter matrices respectively. These matrices are further decomposed as follows;

$$S_{B_s} = \sum_{j=1}^C N_j (M_j - M) U_r U_r^T (M_j - M)^T \quad (8)$$

$$S_{W_s} = \sum_{ij} (x_{ij} - M_j) U_r U_r^T (x_{ij} - M_j)^T \quad (9)$$

where N_j be the total number of samples in j^{th} class, $M = \frac{1}{N} \sum_{ij} \mathbf{x}_{ij}$ is the overall mean matrix and $M_j = \frac{1}{N_j} \sum_{i=1}^{N_j} \mathbf{x}_{ij}$ is the class mean matrix. Analogous to LDA, the solution U_s is given by the eigenvectors of $S_{W_s}^{-1} S_{B_s}$ associated with the q_s largest eigenvalues. By fixing U_s , the solution of the row projection U_r can be obtain similarly. Similar to LDA, the above objective functions (Equations 8 and 9) are further be decomposed into the following two objective functions:

$$S_{GB} = \sum_{j=1}^C N_j U^T (M_j - M) (M_j - M)^T U \quad (10)$$

$$S_{GW} = \sum_{j=1}^C \left(\sum_{i=1}^{K+1} U^T (x_{ij} - M_j) (x_{ij} - M_j)^T U \right) \quad (11)$$

Equation 11 aims to ensure that the samples from the center are as close as possible if and only if they belong to the same class whereas equation 10 makes sure that the center of each class from the total center is as distant as possible. Furthermore, MLDA aims to find projections that maximize the difference between within and between-class scatter. For instance, MLDA learns multi-linear projections alternately and maximizes the following objective function for the column projection:

$$U_s = \operatorname{argmax}_U \left(U^T (S_{B_s} - \xi S_{W_s}) U \right) \quad (12)$$

where ξ is the tuning parameter which is heuristically set to the largest eigenvalue of $(S_{W_s})^{-1} S_{B_s}$. After a simple derivation, the solution U_s is given by the eigenvectors of $S_{B_s} - \xi S_{W_s}$ associated with the q_s largest eigenvalues. By exploiting the tensor structures, MLDA can learn more reliable multi-linear

scatter matrices that have smaller sizes and much better conditioning than LDA. MLDA solves the singularity problem of LDA and gains robustness in estimating global class discriminant information with a small sample size [44]. Equation 12 have a shortcoming, for instance, it may impair the local topology but cannot satisfactorily characterize the local class discriminant information of HSI data. This may lead to instability of within-class compact representation. To overcome these difficulties, this work explicitly computes the local class discriminant information.

3.4 Local Class Discriminant Information

We incorporate the geometrical transformation method which preserves the local class discriminant information by building two adjacency matrices i.e. intrinsic and penalty matrix. The intrinsic matrix characterizes class compactness and connects each sample with its neighboring samples of the same class. While the penalty matrix connects marginal points characterize within class separability. Thus, the objective functions presented in [45] are redefined as follows.

$$U^* = \operatorname{argmax}_U \frac{S_{LB}}{S_{LW}} \quad (13)$$

In which, local within and between class compactness is characterized by the following criteria:

$$S_{LW} = \sum_{i \in S_{k_1}^W(j)} \sum_{j \in S_{k_1}^W(i)} \|U^T \mathbf{x}_i - U^T \mathbf{x}_j\|^2 \quad (14)$$

$$S_{LB} = \sum_{i \in S_{k_2}^B(j)} \sum_{j \in S_{k_2}^B(i)} \|U^T \mathbf{x}_i - U^T \mathbf{x}_j\|^2 \quad (15)$$

$$S_{LW} = 2U^T \mathcal{X}(D^{LW} - W^{LW})\mathcal{X}^T U \quad (16)$$

$$S_{LB} = 2U^T \mathcal{X}(D^{LB} - W^{LB})\mathcal{X}^T U \quad (17)$$

where $S_{k_1}^W(i)$ and $S_{k_2}^B(i)$ indicates the index set of k_1 and k_2 nearest neighbors of \mathbf{x}_i in the same class. D^{LW} and D^{LB} are diagonal matrix whose columns or rows are the sum of W^{LW} and W^{LB} because both are symmetric matrices, e.g. $D_{ii}^{LW} = \sum_j W_{ji}^{LW}$ and $D_{ii}^{LB} = \sum_j W_{ji}^{LB}$. Thus, similar to equations 10 and 11, the equation 13 is decomposed into the following two objective functions.

$$S_{LW} = U^T \mathcal{X}(D^{LW} - W^{LW})\mathcal{X}^T U \quad (18)$$

$$S_{LB} = U^T \mathcal{X}(D^{LB} - W^{LB})\mathcal{X}^T U \quad (19)$$

Equations 18 and 19 are local within and between-class scatters and can characterize the local topology of the samples. Equation 18 aims to make samples compact if and only if they belong to the same class. Equation 19 aims to make them separable if and only if they belong to the different classes. Equations 18 and 19 have a similar problem whereby they only consider local between and within-class scatters but ignore global class discriminant information. It is worth noting that Equation 13 finds the optimal space by maximizing the ratio among within and between-class scatters and to address it, we rewrite equation 13 as follows.

$$\hat{U} = \operatorname{argmax}_U \frac{U^T \mathcal{X}(D^{LB} - W^{LB})\mathcal{X}^T U}{U^T \mathcal{X}(D^{LW} - W^{LW})\mathcal{X}^T U} \quad (20)$$

The optimal projection vector U that maximizes equation 20 is given by the solution of the maximum eigenvalue to the generalized eigenvalue as shown in the following.

$$\mathcal{X}(D^{LB} - W^{LB})\mathcal{X}^T U = \lambda \mathcal{X}(D^{LW} - W^{LW})\mathcal{X}^T U \quad (21)$$

The effectiveness is still limited such as S_{LW} is singular in many cases and the optimal projection cannot be directly calculated. To overcome this problem, we define a novel objective function that jointly considers the total local and global class discriminative information in the following section.

3.5 Objective Function

The parameters $\Omega, \lambda, \Psi = 0.5$ is used to make the trade-off among total within class and total between class scatters and control their proportion as follows.

$$\hat{U} = \operatorname{argmax}_U S(U) \quad (22)$$

$$\hat{U} = \operatorname{argmax}_U (\Omega S_B(U) - (1 - \Omega) S_W(U)) \quad (23)$$

$$S_W(U) = \lambda S_{GW} + (1 - \lambda) S_{LW} \quad (24)$$

$$S_B(U) = \Psi S_{GB} + (1 - \Psi) S_{LB} \quad (25)$$

In above equations $\lambda, \Psi, \Omega = 0.5$ and if $\lambda, \Psi = 0$ the equations 24 and 25 reduces to keep only the local within and between class information. Whereas,

if $\lambda, \Psi = 1$ then the equations 24 and 25 will reduce to keep only global within and between-class scatter information. If $\Omega = 0$, equation 23 reduces to the only total between class scatter whereas, $\Omega = 1$ reduces to the only total within-class scatter. Equation 24 impairs the topological structure of samples and the local within class structure which ignores the global information. To remedy these problems we introduce trade-off coefficient $\Omega = 0.5$ to balance both local and global within class information.

The advantages of this integration are to preserve the global and local within class information in which we can achieve total local class discriminant information. Equation 25 involves the global and local between class information, i.e. relationship among sample centers, but ignores local information e.g. relationship among samples if and only if they belong to a different class. However, a single characterization, either global or local between and within-class may be insufficient, which deteriorates classification performance. This work overcomes the above-said limitation by introducing a discriminative objective function, which preserves both global and local between and within-class scatter information as shown in equation 23. To gain more insight, we solve the equation 23 as follows.

$$\hat{U} = \underset{U}{\operatorname{argmax}} (U^T \mathcal{G} U) \quad (26)$$

where $\mathcal{G} = \Omega \Psi S_B(U) - (1 - \Omega) \lambda S_W(U) + \mathcal{X}[\Omega(1 - \Psi)S_{LB} - (1 - \Omega)(1 - \lambda)S_{LW}] \mathcal{X}^T$, in which D^{LB} and D^{LW} are the Laplacian matrices. Thus, the optimal solution of equation 26 is given by $\operatorname{Max} \operatorname{Tr}\{U^T \mathcal{G} U\}$

with the constraint $U^T U = I$ means the columns of U are orthogonal projection matrix which is able to enhance the discrimination ability among samples and we also used it to reduce the redundancy among the selected samples. Furthermore, we assume that \mathcal{G} is a real symmetric matrix i.e. $\mathcal{G} = \mathcal{G}^T$ because $[\mathcal{X} L^{LB} \mathcal{X}^T]^T = \mathcal{X} L^{LB} \mathcal{X}^T$ and $[\mathcal{X}^T L^{LB} \mathcal{X}]^T = \mathcal{X}^T L^{LB} \mathcal{X}$, moreover, $S_B = S_B^T$ and $S_W = S_W^T$. The complete pipeline of our proposed method is presented in the Algorithm 13 and in Figure 1.

4 EXPERIMENTAL SETTINGS

The Hyperspectral datasets used for experimental purposes belong to the wide variety of classification problems in which the number of classes, number of samples and types of sensors are different, i.e. AVIRIS, ROSIS and Hyperion EO-1 Satellite Sensors. The 5-fold-cross-validation process is

Algorithm 1: Important steps of our proposed AL method.

Data: X_T, X_V

- 1 **Initialization:** $\mathcal{X}, \lambda = 0.5, \Psi = 0.5, \Omega = 0.5;$
- 2 **while** $|X_T| \leq \text{Threshold}$ **do**
- 3 $\mu_{ij} \leftarrow$ Compute the membership matrix;
- 4 $E(\mu) \leftarrow$ Compute the fuzziness;
- 5 $D_V \leftarrow$ Associate the fuzziness, actual and predicted class and spatial information with X_V ;
- 6 Categorize the D_V based on Fuzziness into two groups and sort each group in descending order individually;
- 7 Pick \mathcal{K} misclassified classified samples from each group individually;
- 8 Compute local and global class information for within class scatter $S_W(U) = \lambda S_{GW} + (1 - \lambda) S_{LW}$;
- 9 Compute local and global class information for between class scatter $S_B(U) = \Psi S_{GB} - (1 - \Psi) S_{LB}$;
- 10 Formulate the objective function $\mathcal{G} = \Omega \Psi S_B(U) - (1 - \Omega) \lambda S_W(U) + \mathcal{X}[\Omega(1 - \Psi) S_{LB} - (1 - \Omega)(1 - \lambda) S_{LW}] \mathcal{X}^T$;
- 11 Pick $h \ll \mathcal{K}$ most diverse and spectrally heterogeneous samples from D_V , add them to X_T and remove from X_V ;
- 12 **Repeat until** $|X_T| > \text{Threshold}$;
- 13 **end**

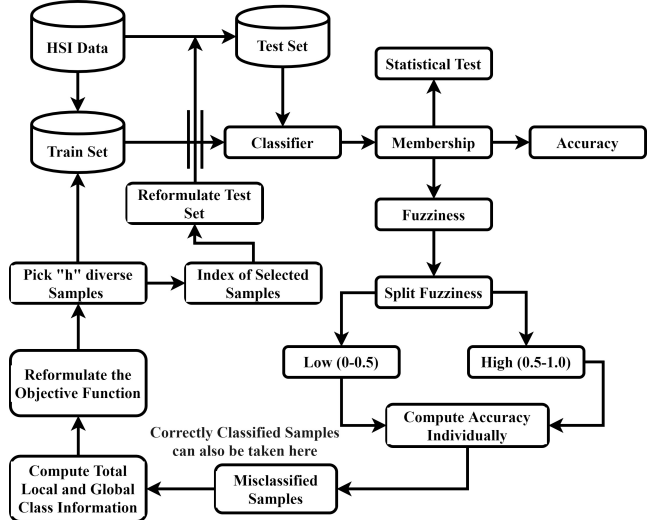


Fig. 1: FLG Flow-Graph: We first compute the fuzziness and then used a divide and conquer strategy to split the fuzziness values into two groups e.g. Low and High Fuzziness. We pick misclassified samples (\mathcal{K}) to compute the global and local class discriminative information and pass this information to the objective function to select ($h \ll \mathcal{K}$) heterogeneous samples.

adopted to evaluate the performance of our proposed pipeline. A necessary normalization between the range of $[0, 1]$ is performed. All the stated experiments are conducted using Matlab 2016b installed

on a Intel inside Core i5 with 8GB RAM.

Experiments have been conducted on several benchmark Hyperspectral datasets using four different types of classifiers, i.e., Support Vector Machine (SVM) [1], K Nearest Neighbours (KNN) [1], Extreme Learning Machine (ELM) [1] and MLR-LORSAL [46] classifiers. All these classifiers are tuned according to the settings mentioned in their respective works. The first goal of this work is to compare the results of all these classifiers on “High” fuzziness samples while considering the total local and global class discriminant information. Later we compare the results of the best classifier on “Low” fuzziness samples again while considering the total local and global class discriminant information. Finally, the complete pipeline is compared with the state-of-the-art AL methods.

For experimental evaluation, several tests have been conducted including but not limited to Kappa (κ), overall accuracy, F1-Score, Precision, and Recall rate. All these evaluation metrics are calculated using the following mathematical formulations.

$$OA = \frac{1}{C} \sum_{i=1}^C TP_i \quad (27)$$

$$\kappa = \frac{P_o - P_e}{1 - P_e} \quad (28)$$

where

$$P_o = \frac{TP + TN}{TP + FN + FP + TN} \quad (29)$$

$$P_e = P_Y + P_N \quad (30)$$

$$P_Y = \frac{TP + FN}{TP + FN + FP + TN} \times \frac{TP + FN}{TP + FN + FP + TN}$$

$$P_N = \frac{FP + TN}{TP + FN + FP + TN} \times \frac{FN + TN}{TP + FN + FP + TN}$$

where TP and FP are true and false positive, TN and FN are true and false negative computed from the confusion matrix.

$$Precision = \frac{1}{C} \sum_{i=1}^C \frac{TP_i}{TP_i + FP_i} \quad (31)$$

$$Recall = \frac{1}{C} \sum_{i=1}^C \frac{TP_i}{TP_i + FN_i} \quad (32)$$

$$F1 - Score = \frac{2 \times (Recall \times Precision)}{(Recall + Precision)} \quad (33)$$

5 EXPERIMENTAL RESULTS

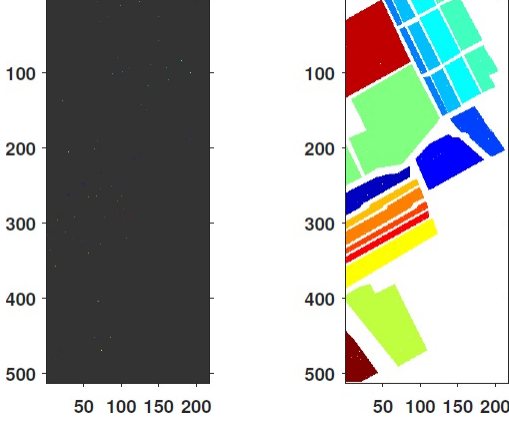
In all these experiments, the initial $n = 50$ training samples are selected randomly and the rest of the samples are used as a test example. We start preserving the total local and global class scatter information from these random samples and later used it for the queried samples. In each iteration of AL, $h = 100$ new samples are selected through the proposed pipeline and added back to the original training set.

5.1 Salinas

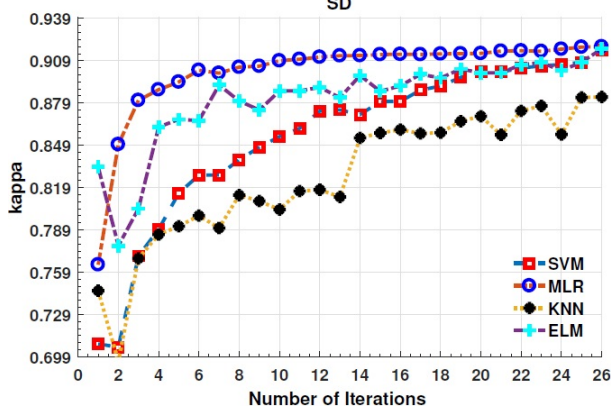
The Salinas dataset (SD) was acquired over Salinas Valley California using AVIRIS sensor. SD is of size $512 \times 217 \times 224$ with a 3.7 meter spatial resolution with 512×217 is spatial and 224 spectral dimensions. SD consists of vineyard fields, vegetables and bare soils. SD consist of 16 classes. A few water absorption bands 108 – 112, 154 – 167 and 224 are removed before analysis. Further details about the dataset can be found at [15]. SD class information is provided in Table 1 and Figure 2 with the respective class accuracies.

TABLE 1: SD Class Description i.e., Class name, Test Samples out of which $n = 50$ as initial and $h = [50 : 100 : 2500]$ in each iteration, as training samples with their respective overall accuracies for SVM, KNN, ELM and MLR-LORSAL Classifiers over 5-cross validation.

Class Names	SVM	KNN	ELM	MLR-LORSAL
Brocoli green weeds 1	0.9654±0.0514	0.9576±0.0555	0.9917±0.0101	0.9831±0.0127
Brocoli green weeds 2	0.9809±0.0295	0.9795±0.0443	0.9947±0.0098	0.9966±0.0040
Fallow	0.9036±0.1097	0.8917±0.1178	0.9480±0.0860	0.9835±0.0335
Fallow rough plow	0.9166±0.0617	0.9883±0.0117	0.9871±0.0126	0.9956±0.0055
Fallow smooth	0.9467±0.0375	0.9423±0.0560	0.9626±0.0773	0.9684±0.0285
Stubble	0.9587±0.1074	0.9918±0.0058	0.9855±0.0503	0.9863±0.0295
Celery	0.9689±0.0285	0.9833±0.0210	0.9975±0.0014	0.9935±0.0050
Grapes untrained	0.7450±0.0863	0.6939±0.1233	0.7768±0.0751	0.8400±0.0465
Soil vineyard develop	0.9666±0.0494	0.9825±0.0192	0.9870±0.0120	0.9953±0.0122
Corn senesced green weeds	0.8799±0.0776	0.8479±0.0704	0.9355±0.0425	0.9236±0.0562
Lettuce romaine 4wk	0.8926±0.0953	0.8535±0.1197	0.9488±0.0366	0.9643±0.0232
Lettuce romaine 5wk	0.9425±0.0767	0.9339±0.0711	0.9602±0.0469	0.9980±0.0040
Lettuce romaine 6wk	0.9633±0.0240	0.9709±0.0203	0.9301±0.0842	0.9909±0.0049
Lettuce romaine 7wk	0.8763±0.0434	0.9173±0.0306	0.9414±0.0333	0.9093±0.0374
Vineyard untrained	0.6907±0.0632	0.5362±0.1116	0.6602±0.1348	0.6950±0.0450
Vineyard vertical trellis	0.9157±0.0875	0.9181±0.1101	0.9718±0.0218	0.9421±0.0783



(a) Initial Train and Test Ground Truths without considering the background pixels in training phase.



(b) Classification Performance of all classifiers.

Fig. 2: Salinas Dataset (SD): Initial Training and Test Ground Truths (Figure 2a) and Classification accuracy with different number of training samples for SVM, KNN, EML and MLR-LORSAL classifiers (Figure 2b).

5.2 Indian Pines Dataset

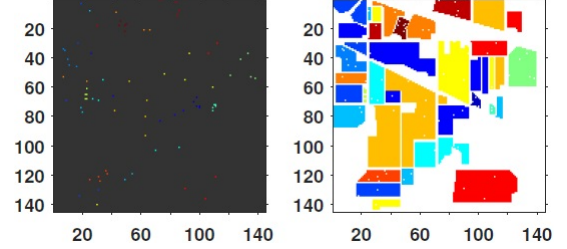
Indian Pines Dataset (IPD) is obtained over north-western Indiana's test site by Airborne Visible / Infrared Imaging Spectrometer (AVIRIS) sensor. IPD is of size $145 \times 145 \times 224$ in the wavelength range $0.4 - 2.5 \times 10^{-6}$ meters where 145×145 is the spatial and 224 spectral dimensions. IPD consists of 1/3 forest and 2/3 agriculture area and other naturally evergreen vegetation. Some crops in the early stages of their growth is also present with approximately less than 5% of total coverage. Low-density housing, building and small roads, Two dual-lane highway and a railway line are also a part of IPD.

The IPD ground truth comprised of 16 classes which are not mutually exclusive. The water absorption bands have been removed before the experiments thus the remaining 200 bands are used

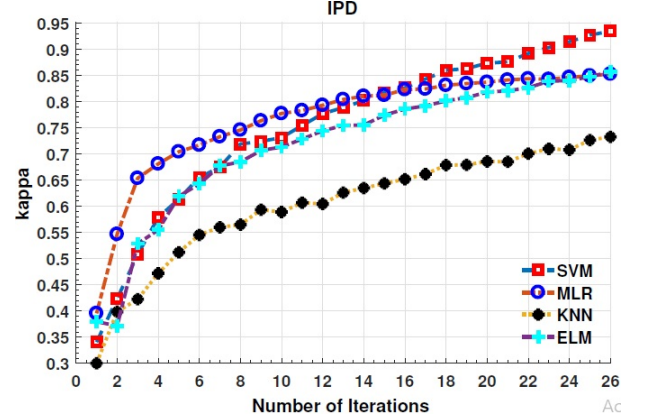
in this experiment. Further details about IPD can be found at [15]. IDP class description is provided in Table 2 and Figure 3 with the respective class accuracies.

TABLE 2: IPD Class Description i.e., Class name, Test Samples out of which $n = 50$ as initial and $h = [50 : 100 : 2500]$ in each iteration, as training samples with their respective κ accuracies for SVM, KNN, ELM and MLR-LORSAL Classifiers over 5-cross validation.

Class Names	SVM	KNN	ELM	MLR-LORSAL
Alfalfa	0.6734 \pm 0.2015	0.4927 \pm 0.1651	0.4107 \pm 0.2475	0.6105 \pm 0.0700
Corn notill	0.7373 \pm 0.1864	0.5469 \pm 0.0790	0.7063 \pm 0.1284	0.7411 \pm 0.1582
Corn mintill	0.6899 \pm 0.1809	0.4650 \pm 0.1370	0.5666 \pm 0.1569	0.6674 \pm 0.1549
Corn	0.5637 \pm 0.2111	0.3783 \pm 0.1238	0.4027 \pm 0.1440	0.5164 \pm 0.1367
Grass pasture	0.8635 \pm 0.1287	0.7596 \pm 0.1817	0.8092 \pm 0.1634	0.8551 \pm 0.0924
Grass trees	0.9003 \pm 0.1277	0.8484 \pm 0.0942	0.9169 \pm 0.0854	0.9450 \pm 0.0675
Grass pasture mowed	0.8726 \pm 0.1019	0.7632 \pm 0.2017	0.4196 \pm 0.1844	0.8899 \pm 0.0502
Hay windrowed	0.9383 \pm 0.0919	0.8452 \pm 0.1554	0.9144 \pm 0.1145	0.9622 \pm 0.0873
Oats	0.7069 \pm 0.1460	0.2724 \pm 0.1430	0.4190 \pm 0.1302	0.7502 \pm 0.0722
Soybean notill	0.7270 \pm 0.1581	0.5610 \pm 0.1441	0.6120 \pm 0.1496	0.7845 \pm 0.0665
Soybean mintill	0.7752 \pm 0.1239	0.6630 \pm 0.0876	0.7670 \pm 0.1011	0.8010 \pm 0.0874
Soybean clean	0.6503 \pm 0.2227	0.3689 \pm 0.1280	0.6278 \pm 0.2022	0.6911 \pm 0.1367
Wheat	0.9571 \pm 0.0437	0.8785 \pm 0.1119	0.9451 \pm 0.0648	0.9484 \pm 0.0772
Woods	0.8795 \pm 0.0967	0.8668 \pm 0.1122	0.9141 \pm 0.1045	0.9419 \pm 0.0565
Buildings Grass Trees Drives	0.7082 \pm 0.1496	0.3949 \pm 0.1245	0.6854 \pm 0.1820	0.4994 \pm 0.0842
Stone Steel Towers	0.8331 \pm 0.0938	0.8265 \pm 0.0413	0.7773 \pm 0.0813	0.8379 \pm 0.0336



(a) Initial Train and Test Ground Truths without considering the background pixels in training phase.



(b) Classification Performance of all classifiers.

Fig. 3: Indian Pines Dataset (IPD): Initial Training and Test Ground Truths (Figure 3a) and Classification accuracy with different number of training samples for SVM, KNN, EML and MLR-LORSAL classifiers (Figure 3b).

5.3 Kennedy Space Center

Kennedy Space Center dataset (KSCD) acquired on March 23, 1996 using NASA AVIRIS instrument over Kennedy Space Center, Florida. KSCD consists of 224 spectral bands of 10 nm in the wavelength range 400–2500 nm with 18 meter spatial resolution from an altitude of 20 km. 176 out of 224 bands are used for the experimental purposes and remaining water absorption and low SNR bands have been removed. KSCD consist of 13 classes. KSCD class information is provided in Table 3 and Figure 4 with the respective class accuracies.

TABLE 3: KSCD Class Description i.e., Class name, Test Samples out of which $n = 50$ as initial and $h = [50 : 100 : 2500]$ in each iteration, as training samples with their respective κ accuracies for SVM, KNN, ELM and MLR-LORSAL Classifiers over 5-cross validation.

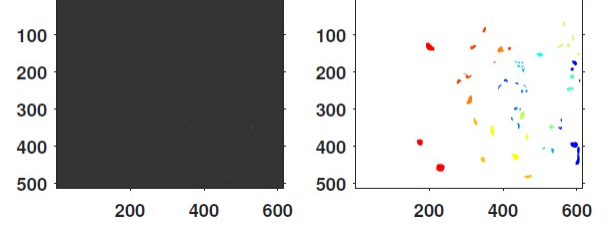
Class Names	SVM	KNN	ELM	MLR-LORSAL
Scrub	0.9422±0.1953	0.9692±0.0588	0.9588±0.0742	0.9305±0.1339
Willow Swamp	0.9386±0.1968	0.9276±0.1392	0.9601±0.0721	0.9263±0.0528
CP/Oak	0.9365±0.1958	0.9495±0.1186	0.9170±0.1198	0.8408±0.1918
CP hammock	0.8864±0.2254	0.8785±0.2113	0.8075±0.2008	0.6052±0.0952
Slash Pine	0.9002±0.2101	0.8701±0.1955	0.8428±0.1902	0.4006±0.1145
Oak/Broadleaf	0.8734±0.2383	0.8362±0.2378	0.7992±0.1999	0.5197±0.0910
Hardwood Swamp	0.9115±0.2036	0.9167±0.1507	0.9010±0.1360	0.7055±0.1347
Graminoid Marsh	0.9312±0.2034	0.9253±0.1729	0.9385±0.0869	0.7754±0.1620
Spartina Marsh	0.9427±0.1978	0.9589±0.0969	0.9553±0.0852	0.8852±0.0334
Cattail Marsh	0.9443±0.1992	0.9355±0.1601	0.9800±0.0288	0.8900±0.1807
Salt Marsh	0.9331±0.1989	0.9858±0.0327	0.9820±0.0351	0.9404±0.0346
Mud Flats	0.9406±0.1990	0.9371±0.1216	0.9460±0.0742	0.8467±0.0378
Water	0.9587±0.1956	0.9980±0.0053	0.9961±0.0067	0.9502±0.1939

5.4 Botswana

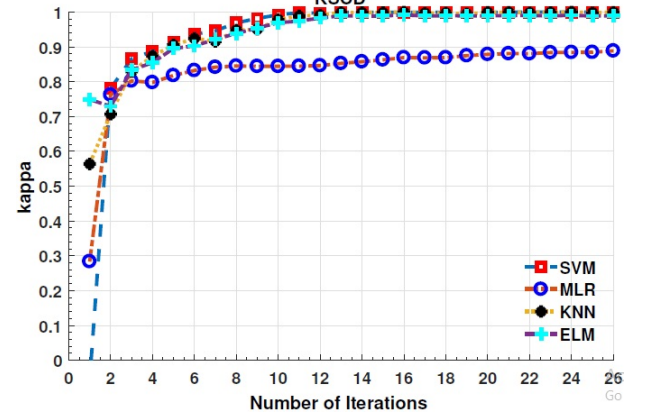
Botswana Dataset (BSD) acquired over the Okavango Delta, Botswana on May 31, 2001 through a Hyperion sensor mounted on NASA EO – 1 Satellite. BSD consists of 242 bands of 10nm in the wavelength range of 400 – 2500 nm with a 30 meter spatial resolution from an altitude of 7.7 km. The number of bands reduced to 145 from 242 by removing noisy and uncalibrated bands. The total ground truth classes are 14 that represent occasional swamps, drier woodlands and seasonal swamps. BSD class information is provided in Table 4 and Figure 5 with the respective class accuracies.

5.5 Pavia University

Pavia University Dataset (PUD) gathered over Pavia in northern Italy using a Reflective Optics System Imaging Spectrometer (ROSIS) optical sensor. PUD consists of 610×610 spatial and 103 spectral bands with a spatial resolution of 1.3 meters. PUD ground truth classes are 9. PUD class information is provided in Table 5 and Figure 6 with the respective class accuracies.



(a) Initial Train and Test Ground Truths without considering the background pixels in training phase.



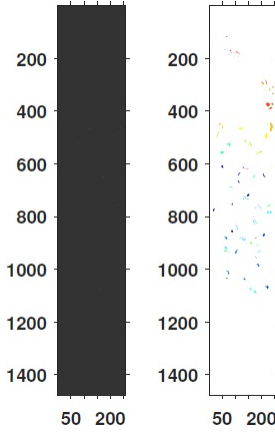
(b) Classification Performance of all classifiers.

Fig. 4: Kennedy Space Center Dataset (KSCD): Initial Training and Test Ground Truths (Figure 4a) and Classification accuracy with different number of training samples for SVM, KNN, EML and MLR-LORSAL classifiers (Figure 4b).

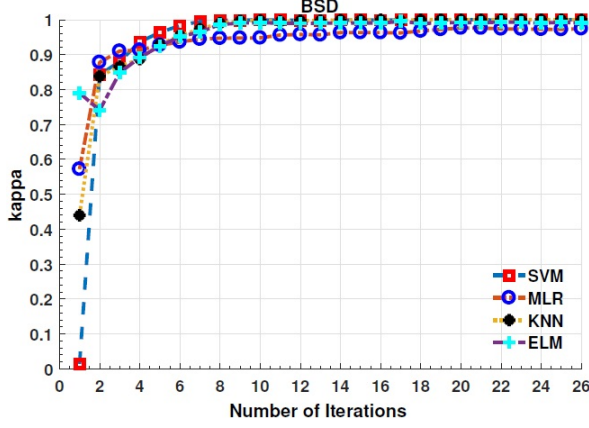
TABLE 4: BSD Class Description i.e., Class name, Test Samples out of which $n = 50$ as initial and $h = [50 : 100 : 2500]$ in each iteration, as training samples with their respective κ accuracies for SVM, KNN, ELM and MLR-LORSAL Classifiers over 5-cross validation.

Class Names	SVM	KNN	ELM	MLR-LORSAL
Water	0.9525±0.1966	0.9994±0.0030	0.9994±0.0023	0.9994±0.0030
Hippo Grass	0.9533±0.1352	0.9719±0.0862	0.9776±0.0437	0.9928±0.0347
Floodplain Grasses 1	0.9890±0.0439	0.9793±0.0536	0.9757±0.0579	0.9873±0.0474
Floodplain Grasses 2	0.9544±0.1954	0.9660±0.1174	0.9742±0.0672	0.9773±0.0741
Reeds 1	0.9419±0.1982	0.9362±0.1421	0.9517±0.0824	0.8883±0.0965
Riparian	0.9239±0.2141	0.8949±0.2183	0.9002±0.1634	0.8239±0.1546
Firescar 2	0.9573±0.1956	0.9715±0.1141	0.9907±0.0233	0.9687±0.1040
Island Interior	0.9581±0.1956	0.9672±0.1026	0.9758±0.0555	0.9837±0.0771
Acacia Woodlands	0.9494±0.1955	0.9371±0.1510	0.9464±0.0902	0.9298±0.1032
Acacia Shrublands	0.9474±0.1968	0.9577±0.1026	0.9264±0.0876	0.9464±0.0648
Acacia Grasslands	0.9419±0.2000	0.9624±0.1109	0.9664±0.0609	0.9283±0.0960
Short Mopane	0.9502±0.1955	0.9684±0.0934	0.9632±0.0723	0.9369±0.0137
Mixed Mopane	0.9507±0.1961	0.9524±0.1331	0.9457±0.1202	0.9418±0.0643
Exposed Soils	0.9229±0.2124	0.9948±0.0141	0.9789±0.0396	0.9776±0.0847

Here we enlist the experimental results obtained in each iteration of the proposed AL framework for four different types of classifiers, i.e., SVM, KNN, ELM, and MLR-LORSAL. These classifiers have been rigorously used in the literature for comparative analysis. The comparative performance of our proposed AL pipeline using the aforementioned



(a) Initial Train and Test Ground Truths without considering the background pixels in training phase.



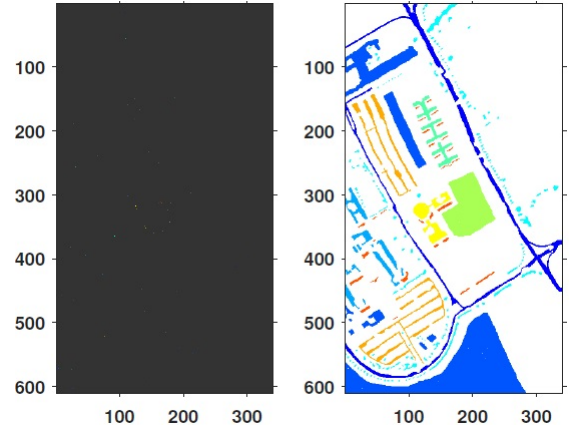
(b) Classification Performance of all classifiers.

Fig. 5: Botswana Dataset (BSD): Initial Training and Test Ground Truths (Figure 5a) and Classification accuracy with different number of training samples for SVM, KNN, EML and MLR-LORSAL classifiers (Figure 5b).

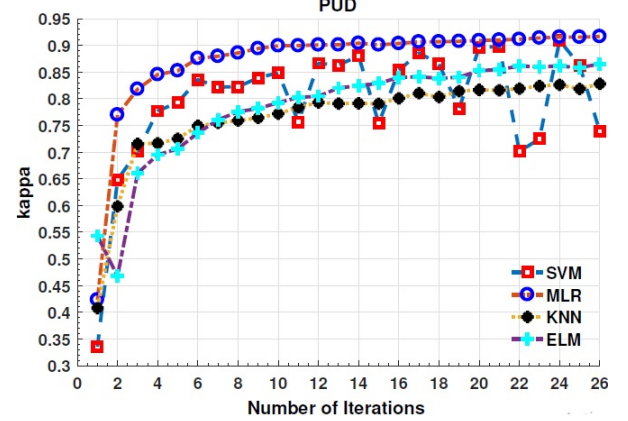
TABLE 5: PUD Class Description i.e., Class name, Test Samples out of which $n = 50$ as initial and $h = [50 : 100 : 2500]$ in each iteration, as training samples with their respective κ accuracies for SVM, KNN, ELM and MLR-LORSAL Classifiers over 5-cross validation.

Class Names	SVM	KNN	ELM	MLR-LORSAL
Asphalt	0.7802 \pm 0.1752	0.8431 \pm 0.0752	0.8528 \pm 0.0610	0.8788 \pm 0.0653
Meadows	0.9082 \pm 0.1252	0.8942 \pm 0.0646	0.9072 \pm 0.0765	0.9537 \pm 0.0904
Gravel	0.6901 \pm 0.0876	0.6305 \pm 0.1082	0.6175 \pm 0.1200	0.7033 \pm 0.0738
Trees	0.8564 \pm 0.1006	0.8124 \pm 0.0652	0.8698 \pm 0.0844	0.8817 \pm 0.0763
Painted metal sheets	0.9032 \pm 0.1690	0.9776 \pm 0.0583	0.8081 \pm 0.1712	0.9532 \pm 0.1153
Bare Soil	0.8052 \pm 0.1344	0.6141 \pm 0.1344	0.7221 \pm 0.1372	0.8486 \pm 0.1420
Bitumen	0.7439 \pm 0.1138	0.6942 \pm 0.0954	0.6106 \pm 0.1607	0.8191 \pm 0.0357
Self-Blocking Bricks	0.7562 \pm 0.0927	0.7588 \pm 0.1271	0.7415 \pm 0.1282	0.8759 \pm 0.0470
Shadows	0.7950 \pm 0.1790	0.9981 \pm 0.0018	0.9945 \pm 0.0101	0.9972 \pm 0.0060

classifiers has been shown in Figures 2-6. The tuning parameters of all the above-said classifiers have been explored very carefully in the first few experiments and chosen those which provide the best



(a) Initial Train and Test Ground Truths without considering the background pixels in training phase.



(b) Classification Performance of all classifiers.

Fig. 6: Pavia University Dataset (PUD): Initial Training and Test Ground Truths (Figure 6a) and Classification accuracy with different number of training samples for SVM, KNN, EML and MLR-LORSAL classifiers (Figure 6b).

accuracy. To avoid bias, all the listed experiments are carried out in the same settings on the same machine. Before the experiments, we performed the necessary normalization between $[0, 1]$ and all the experiments are carried out using Matlab 2016b installed on an Intel inside Core i5 with 8GB RAM.

Here we also enlisted the computational time for SVM, KNN, ELM and MLR-LORSAL classifiers in Figure 7. One can observe that the computational time is gradually increasing as the number of training samples increases for all classifiers except for the KNN classifier which exponentially increases. However, the trend is quite different for accuracy which increases exponentially for all classifiers as compared to the time. Computational complexity can significantly reduce for KNN classifiers while using any optimization methods. In our case, we

TABLE 6: Statistical Significance of our proposed Pipeline.

Dataset	SVM			KNN			ELM			MLR-LORSAL		
	Recall	Precision	F1-Score	Recall	Precision	F1-Score	Recall	Precision	F1-Score	Recall	Precision	F1-Score
SD	0.9071±0.0114	0.9213±0.0133	0.9122±0.0119	0.8993±0.0166	0.9009±0.0158	0.8978±0.0159	0.9362±0.0122	0.9387±0.0122	0.9359±0.0119	0.9478±0.0101	0.9443±0.0089	0.9454±0.0093
KSCD	0.9261±0.0046	0.9612±0.0056	0.9243±0.0046	0.9299±0.0087	0.9306±0.0082	0.9282±0.0079	0.9219±0.0122	0.9271±0.0113	0.9210±0.0109	0.7859±0.0288	0.8062±0.0233	0.7877±0.0255
IPD	0.7798±0.0161	0.7715±0.0174	0.7679±0.0158	0.6207±0.0284	0.6357±0.0280	0.6074±0.0269	0.6809±0.0272	0.7720±0.0222	0.6986±0.0245	0.7776±0.0201	0.7546±0.0192	0.7529±0.0181
BSD	0.9495±0.0036	0.9862±0.0018	0.9484±0.0023	0.9614±0.0042	0.9627±0.0045	0.9606±0.0040	0.9623±0.0052	0.9661±0.0052	0.9629±0.0047	0.9487±0.0075	0.9471±0.0067	0.9467±0.0065
PUD	0.8043±0.0256	0.8150±0.0328	0.7980±0.0273	0.8025±0.0325	0.8077±0.0328	0.8021±0.0320	0.7916±0.0317	0.8147±0.0326	0.7974±0.0312	0.8791±0.0209	0.8852±0.0200	0.8799±0.0191

retrain KNN classifier for $k = [2 - 20]$ in each iteration, which can be overcome using a grid-search type method. All other classifiers have less computational cost and better accuracies, however, SVM and MLR-LORSAL have higher generalization performance then ELM followed by KNN.

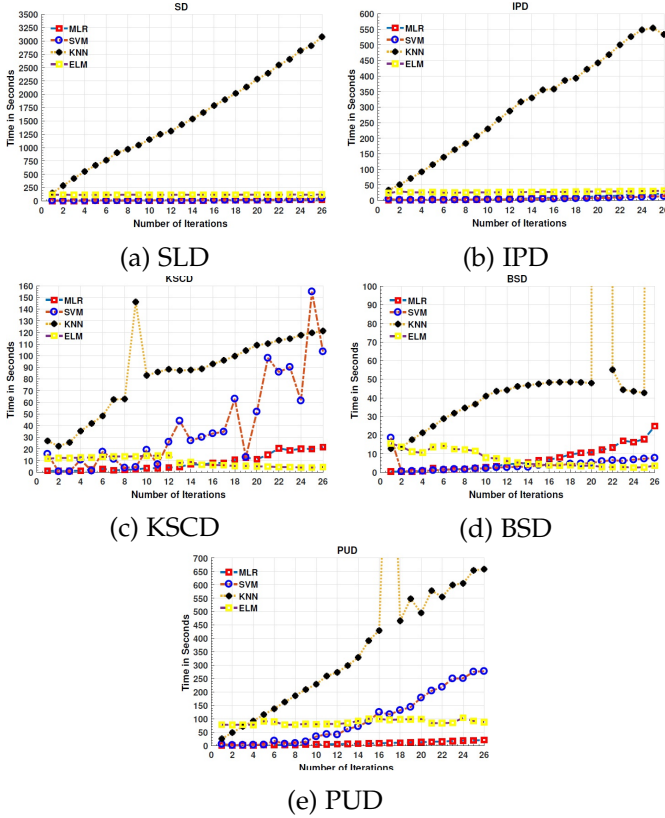


Fig. 7: Computational Time for all classifiers for each dataset used in this work.

The results shown in the above Figures and Tables are based on 5 Monte Carlo runs with a different number of training samples with equal class representation and in each iteration, the training set size is increased with $h = 100$ of selected samples by our proposed pipeline. It is perceived from Figures and Tables that by including the samples back to the training set, the classification results are significantly improved for all the classifiers and datasets. Moreover, it can be seen that all the classifiers are robust except KNN and their generalization has been significantly increased as shown in Table 6.

In this work, we start evaluating our hypotheses from $n = 50$ number of randomly selected labeled training samples and we demonstrate that adding more samples back into the training set significantly increases the accuracy. It is worth noting from experiments that the classifiers trained with selected samples produce better accuracy and improve the generalization performance on those samples which were initially misclassified. To experimentally observe a sufficient quantity of labeled training samples for each classifier, we evaluated the hypotheses with a different number of labeled training samples. Based on the experimental results we conclude that $h = 400 - 600$ samples obtained by FLG are good enough to produce the acceptable accuracy for Hyperspectral Image Classification.

6 CONCLUSION

In this paper, a fuzziness-based total local and global class discriminant information preserving active learning method is proposed for HSIC. In this line of investigation, a classifier is trained with a very small set of labeled training samples and evaluated on a large number of unlabeled samples. From results, we observe that it is enough to create a classification model from a small sample instead of a complex model with too many labeled training samples and parameters. Moreover, a small portion of unlabeled samples selected from high fuzziness group to train the model can enhance the generalization performance of any classifier.

The classification results obtained with a different number of labeled training samples prove that the selection of initial labeled training samples does not affect FLG labeling success and does not influence the final classification accuracies. The experimental results show that the FLG which exploits both labeled and unlabeled samples information performs better than standard methods that use only uncertainty information, especially with small sample sizes.

REFERENCES

- [1] M. Ahmad, A. Khan, A. Khan, M. Mazzara, S. Distefano, A. Sohaib, and O. Nibouche, "Spatial prior fuzziness pool-

- based interactive classification of hyperspectral images," *Remote Sensing*, vol. 11, no. 5, May. 2019.
- [2] Z. Ding, N. Qi, F. Dong, L. Jinhui, Y. Wei, and Y. Shenggui, "Application of multispectral remote sensing technology in surface water body extraction," in *2016 International Conference on Audio, Language and Image Processing (ICALIP)*, July 2016, pp. 141–144.
 - [3] M. Ahmad, M. A. Alqarni, A. M. Khan, R. Hussain, M. Mazzara, and S. Distefano, "Segmented and non-segmented stacked denoising autoencoder for hyperspectral band reduction," *Optik - International Journal for Light and Electron Optics*, vol. 180, pp. 370–378, Oct 2018.
 - [4] F. Melgani and L. Bruzzone, "Classification of hyperspectral remote sensing images with support vector machines," *IEEE Transactions on Geoscience and Remote Sensing*, vol. 42, no. 8, pp. 1778–1790, August 2004.
 - [5] M. S. Aydemir and G. Bilgin, "Semi supervised hyperspectral image classification using small sample sizes," *IEEE Geoscience and Remote Sensing Letters*, vol. 14, no. 5, pp. 621–625, May 2017.
 - [6] C. Deng, X. Liu, C. Li, and D. Tao, "Active multi-kernel domain adaptation for hyperspectral image classification," *Pattern Recogn.*, vol. 77, no. C, pp. 306–315, May 2018. [Online]. Available: <https://doi.org/10.1016/j.patcog.2017.10.007>
 - [7] M. Ahmad, S. Protasov, A. M. Khan, R. Hussain, A. M. Khattak, and W. A. Khan, "Fuzziness-based active learning framework to enhance hyperspectral image classification performance for discriminative and generative classifiers," *PLoS ONE*, vol. 13, no. 1, p. e0188996, January 2018.
 - [8] M. Ahmad, S. Lee, D. Ulhaq, and Q. Mushtaq, "Hyperspectral remote sensing: Dimensional reduction and end member extraction," *International Journal of Soft Computing and Engineering (IJSCE)*, vol. 2, pp. 2231–2307, 05 2012.
 - [9] M. Ahmad, A. M. Khan, and R. Hussain, "Graph-based spatial spectral feature learning for hyperspectral image classification," *IET Image Processing*, vol. 11, no. 12, pp. 1310–1316, 2017.
 - [10] M. Ahmad, D. Ulhaq, Q. Mushtaq, and M. Sohaib, "A new statistical approach for band clustering and band selection using k-means clustering," *International Journal of Engineering and Technology*, vol. 3, pp. 606–614, 12 2011.
 - [11] M. Ahmad, D. Ihsan, and D. Ulhaq, "Linear unmixing and target detection of hyperspectral imagery using osp," in *International Proceedings of Computer Science and Information Technology*, 01 2011, pp. 179–183.
 - [12] M. Ahmad, D. Ulhaq, and Q. Mushtaq, "Aik method for band clustering using statistics of correlation and dispersion matrix," in *International Conference on Information Communication and Management*, 01 2011, pp. 114–118.
 - [13] M. Chi and L. Bruzzone, "Semi supervised classification of hyperspectral images by svms optimized in the primal," *IEEE Transactions on Geoscience and Remote Sensing*, vol. 45, no. 6, pp. 1870–1880, June 2007.
 - [14] L. Mingkun and I. K. Sethi, "Confidence-based active learning," *IEEE Transactions on Pattern Analysis and Machine Intelligence*, vol. 28, no. 8, pp. 1251–1261, Aug 2006.
 - [15] M. Ahmad, S. Shabbir, D. Oliva, M. Mazzara, and S. Distefano, "Spatial-prior generalized fuzziness extreme learning machine autoencoder-based active learning for hyperspectral image classification," *Optik*, vol. 206, p. 163712, 2020. [Online]. Available: <http://www.sciencedirect.com/science/article/pii/S0030402619316109>
 - [16] D. D. Lewis and W. A. Gale, "A sequential algorithm for training text classifiers," in *Proceedings of the 17th Annual International ACM SIGIR Conference on Research and Development in Information Retrieval*, ser. SIGIR '94. New York, NY, USA: Springer-Verlag New York, Inc., 1994, pp. 3–12. [Online]. Available: <http://dl.acm.org/citation.cfm?id=188490.188495>
 - [17] B. Settles, "Active learning literature survey," University of Wisconsin, Madison, WI, USA, Tech. Rep., 2010.
 - [18] H. S. Seung, M. Oppor, and H. Sompolinsky, "Query by committee," in *Proceedings of the Fifth Annual Workshop on Computational Learning Theory*, ser. COLT'92. New York, NY, USA: ACM, 1992, pp. 287–294. [Online]. Available: <http://doi.acm.org/10.1145/130385.130417>
 - [19] D. Tuia, M. Volpi, L. Copa, M. Kanevski, and J. Munoz-Mari, "A survey of active learning algorithms for supervised remote sensing image classification," *IEEE Journal of Selected Topics in Signal Processing*, vol. 5, no. 3, pp. 606–617, June 2011.
 - [20] D. Liu, X.-S. Hua, L. Yang, and H.-J. Zhang, "Multiple-instance active learning for image categorization," in *Advances in Multimedia Modeling*. Berlin, Heidelberg: Springer Berlin Heidelberg, 2009, pp. 239–249.
 - [21] D. A. Cohn, Z. Ghahramani, and M. I. Jordan, "Active learning with statistical models," *J. Artif. Int. Res.*, vol. 4, no. 1, pp. 129–145, Mar. 1996. [Online]. Available: <http://dl.acm.org/citation.cfm?id=1622737.1622744>
 - [22] X. Zhu, "Semi-supervised learning with graphs," Ph.D. dissertation, Language Technologies Institute, School of Computer Science, Carnegie Mellon University, Pittsburgh, PA, USA, 2005, aAI3179046.
 - [23] A. McCallum and K. Nigam, "Employing em and pool-based active learning for text classification," in *Proceedings of the Fifteenth International Conference on Machine Learning*, ser. ICML '98. San Francisco, CA, USA: Morgan Kaufmann Publishers Inc., 1998, pp. 350–358. [Online]. Available: <http://dl.acm.org/citation.cfm?id=645527.757765>
 - [24] L. Zhang, C. Chen, J. Bu, D. Cai, X. He, and T. S. Huang, "Active learning based on locally linear reconstruction," *IEEE Transactions on Pattern Analysis and Machine Intelligence*, vol. 33, no. 10, pp. 2026–2038, Oct 2011.
 - [25] X. Zuobing, A. Ram, and Z. Yi, "Incorporating diversity and density in active learning for relevance feedback," in *European Conference on Information Retrieval Advances in Information Retrieval (ECIR 2007)*, July 2007, pp. 246–257.
 - [26] B. Settles and M. Craven, "An analysis of active learning strategies for sequence labeling tasks," in *Proceedings of the Conference on Empirical Methods in Natural Language Processing*, ser. EMNLP'08. Stroudsburg, PA, USA: Association for Computational Linguistics, 2008, pp. 1070–1079. [Online]. Available: <http://dl.acm.org/citation.cfm?id=1613715.1613855>
 - [27] J. Li, J. M. Bioucas-Dias, and A. Plaza, "Semi supervised hyperspectral image segmentation using multinomial logistic regression with active learning," *IEEE Transactions on Geoscience and Remote Sensing*, vol. 48, no. 11, pp. 4085–4098, Nov 2010.
 - [28] L. Z. Huo and P. Tang, "A batch-mode active learning algorithm using region-partitioning diversity for svm classifier," *IEEE Journal of Selected Topics in Applied Earth Observations and Remote Sensing*, vol. 7, no. 4, pp. 1036–1046, April 2014.
 - [29] E. Pasolli, F. Melgani, N. Alajlan, and Y. Bazi, "Active learning methods for biophysical parameter estimation,"

- IEEE Transactions on Geoscience and Remote Sensing*, vol. 50, no. 10, pp. 4071–4084, Oct 2012.
- [30] N. Rubens, M. Elahi, M. Sugiyama, and D. Kaplan, *Active Learning in Recommender Systems*, 2nd ed. Springer Verlag Boston, MA, 2015.
- [31] M. Pabitra, U. Shankar, and S. K. Pal, “Segmentation of multispectral remote sensing images using active support vector machines,” *Pattern Recognition Letters*, vol. 25, no. 9, pp. 1067–1074, July 2004.
- [32] J. Li, J. M. Bioucas-Dias, and A. Plaza, “Spectral spatial classification of hyperspectral data using loopy belief propagation and active learning,” *IEEE Transactions on Geoscience and Remote Sensing*, vol. 51, no. 2, pp. 844–856, Feb 2013.
- [33] L. Tong, K. Kramer, S. Samson, A. Remsen, D. B. Goldgof, L. O. Hall, and T. Hopkins, “Active learning to recognize multiple types of plankton,” in *Proceedings of the 17th International Conference on Pattern Recognition, 2004. ICPR 2004.*, vol. 3, Aug 2004, pp. 478–481 Vol.3.
- [34] Q. Shi, B. Du, and L. Zhang, “Spatial coherence-based batch-mode active learning for remote sensing image classification,” *IEEE Transactions on Image Processing*, vol. 24, no. 7, pp. 2037–2050, July 2015.
- [35] H. Yu, X. Yang, S. Zheng, and C. Sun, “Active learning from imbalanced data: A solution of online weighted extreme learning machine,” *IEEE Transactions on Neural Networks and Learning Systems*, pp. 1–16, 2018.
- [36] M. Ahmad, A. Khan, and A. K. Bashir, “Metric similarity regularizer to enhance pixel similarity performance for hyperspectral unmixing,” *Optik - International Journal for Light and Electron Optics*, vol. 140, no. C, pp. 86–95, July 2017.
- [37] M. Ahmad, A. M. Khan, R. Hussain, S. Protasov, F. Chow, and A. M. Khattak, “Unsupervised geometrical feature learning from hyperspectral data,” in *2016 IEEE Symposium Series on Computational Intelligence (IEEE SSCI 2016)*, December 2016, pp. 1–6.
- [38] M. Ahmad, S. Protasov, and A. M. Khan, “Hyperspectral band selection using unsupervised non-linear deep auto encoder to train external classifiers,” *CoRR*, vol. abs/1705.06920, 2017. [Online]. Available: <http://arxiv.org/abs/1705.06920>
- [39] G. Quanxue, L. Jingjing, Z. Haijun, H. Jun, and Y. Xiaojing, “Two-dimensional supervised local similarity and diversity projection,” *Pattern Recognition*, vol. 45, no. 10, pp. 3717–3724, October 2012. [Online]. Available: <https://doi.org/10.1016/j.patcog.2012.03.024>
- [40] A. Sharma and K. Paliwal, “Linear discriminant analysis for the small sample size problem: an overview,” *International Journal of Machine Learning and Cybernetics*, vol. 6, p. 443–454, 06 2014.
- [41] S. Prince, P. Li, Y. Fu, U. Mohammed, and J. Elder, “Probabilistic models for inference about identity,” *IEEE Transactions on Pattern Analysis and Machine Intelligence*, vol. 34, no. 1, pp. 144–157, Jan 2012.
- [42] H. Lu, K. N. Plataniotis, and A. N. Venetsanopoulos, “Uncorrelated multilinear discriminant analysis with regularization and aggregation for tensor object recognition,” *IEEE Transactions on Neural Networks*, vol. 20, no. 1, pp. 103–123, Jan 2009.
- [43] D. Tao, X. Li, X. Wu, and S. Maybank, “Tensor rank one discriminant analysis—a convergent method for discriminative multilinear subspace selection,” *Neurocomput.*, vol. 71, no. 10–12, pp. 1866–1882, Jun. 2008. [Online]. Available: <http://dx.doi.org/10.1016/j.neucom.2007.08.036>
- [44] L. Dijun, C. Ding, and H. Huang, “Symmetric two dimensional linear discriminant analysis (2dlda),” in *2009 IEEE Conference on Computer Vision and Pattern Recognition*, June 2009, pp. 2820–2827.
- [45] D. Chuntao and Z. Li, “Double adjacency graphs-based discriminant neighborhood embedding,” *Pattern Recognition*, vol. 48, no. 5, pp. 1734–1742, May 2015.
- [46] I. Dopido, J. Li, A. Plaza, and J. M. Bioucas-Dias, “A new semi-supervised approach for hyperspectral image classification with different active learning strategies,” in *2012 4th Workshop on Hyperspectral Image and Signal Processing: Evolution in Remote Sensing (WHISPERS)*, 2012, pp. 1–4.